

1 **Surface ozone and its precursors at Summit, Greenland: comparison between observations**
2 **and model simulations**

3 Yaoxian Huang^{1,a}, Shiliang Wu^{1,2,3}, Louisa J. Kramer^{1,2,b}, Detlev Helmig⁴, and Richard E.
4 Honrath^{1,2,†}

5 ¹Department of Geological and Mining Engineering and Sciences, Michigan Technological
6 University, Houghton, Michigan, USA

7 ²Atmospheric Sciences Program, Michigan Technological University, Houghton, Michigan,
8 USA

9 ³College of Environmental Science and Engineering, Ocean University of China, Qingdao, China

10 ⁴Institute of Arctic and Alpine Research, University of Colorado, Boulder, Colorado, USA

11 ^anow at: Department of Climate and Space Sciences and Engineering, University of Michigan,
12 Ann Arbor, Michigan, USA

13 ^bnow at: University of Birmingham, Birmingham, UK

14 [†]deceased

15
16 *Correspondence to:* S. Wu (slwu@mtu.edu) and Y. Huang (yaoxianh@mtu.edu)
17

18 **Abstract.** Recent studies have shown significant challenges for atmospheric models to simulate
19 tropospheric ozone (O₃) and its precursors in the Arctic. In this study, ground based data were
20 combined with a global 3-D chemical transport model (GEOS-Chem) to examine the abundance
21 and seasonal variations of O₃ and its precursors at Summit, Greenland (72.34° N, 38.29° W, 3212
22 m.a.s.l). Model simulations for atmospheric nitrogen oxides (NO_x), peroxyacetyl nitrate (PAN),
23 ethane (C₂H₆), propane (C₃H₈), carbon monoxide (CO), and O₃ for the period of 07/2008-
24 06/2010 were compared with observations. The model performed well in simulating certain
25 species (such as CO and C₃H₈), but some significant discrepancies were identified for other
26 species and further investigated. The model generally underestimated NO_x and PAN (by ~ 50%
27 and 30%, respectively) for March-June. Likely contributing factors to the low bias include
28 missing NO_x and PAN emissions from snowpack chemistry in the model. At the same time, the
29 model overestimated NO_x mixing ratios by more than a factor of two in wintertime, with
30 episodic NO_x mixing ratios up to 15 times higher than the typical NO_x levels at Summit. Further
31 investigation showed that these simulated episodic NO_x spikes were always associated with
32 transport events from Europe, but the exact cause remained unclear. The model systematically
33 overestimated C₂H₆ mixing ratios by approximately 20% relative to observations. This

34 discrepancy can be resolved by decreasing anthropogenic C₂H₆ emissions over Asia and the US
35 by ~ 20%, from 5.4 to 4.4 Tg/yr. GEOS-Chem was able to reproduce the seasonal variability of
36 O₃ and its spring maximum. However, compared with observations, it underestimated surface O₃
37 by approximately 13% (6.5 ppbv) from April to July. This low bias appeared to be driven by
38 several factors including missing snowpack emissions of NO_x and nitrous acid in the model, the
39 weak simulated stratosphere-to-troposphere exchange flux of O₃ over the summit, as well as the
40 coarse model resolution.

41 **1. Introduction**

42 Tropospheric ozone (O₃) and its precursors, including nitrogen oxides (NO_x = NO + NO₂),
43 carbon monoxide (CO), and volatile organic compounds (VOCs, such as ethane, propane, etc.)
44 are important atmospheric species affecting both air quality and climate (e.g., Jacob et al., 1992;
45 Fiore et al., 2002; Unger et al., 2006; Hollaway et al., 2012). Tropospheric O₃ is mainly
46 produced by photochemical oxidation of CO and VOCs in the presence of NO_x, with additional
47 contribution by transport from the stratosphere. Its major sinks include chemical reactions and
48 dry deposition. As a reservoir species for NO_x, peroxyacetyl nitrate (PAN) also plays an
49 important role in atmospheric chemistry. PAN and O₃, as well as some of their precursors, have
50 relatively long lifetimes in the atmosphere, enabling them to be transported long distance to
51 remote regions such as the Arctic.

52 Recent studies have shown some significant challenges for atmospheric chemical transport
53 models to simulate O₃ and its precursors in the Arctic (e.g., Shindell et al., 2008; Alvarado et al.,
54 2010; Walker et al., 2012; Wespes et al., 2012; Fischer et al., 2014; Monks et al., 2015), but the
55 causes remain unclear. In the multi-model assessment by Shindell et al. (2008), more than a
56 dozen models all showed systematic and persistent underestimation of O₃ at the GEOSummit
57 station, Greenland (hereafter referred to as Summit). Alvarado et al. (2010) used NO_x and PAN
58 measurements from the ARCTAS (Arctic Research of the Composition of the Troposphere from
59 Aircraft and Satellites) mission in the summer to compare with model simulations. They found
60 that model simulated NO_x mixing ratios were higher than observations, while PAN mixing ratios
61 were lower than the observations in fresh boreal fire plumes. In terms of global PAN
62 simulations, Fischer et al. (2014) directly partitioned 40% of NO_x emissions from wildfires to
63 PAN formation, which improved the agreement between model and observations. However, the

64 model still underestimated PAN surface mixing ratios during springtime in the Arctic. Walker et
65 al. (2012) reported that model simulated O₃ mixing ratios were biased low when compared with
66 balloon data during summertime from two high-latitude sites at Eureka (80°N, 86°W) and Ny-
67 Ålesund (79°, 12°E). Wespes et al. (2012) also revealed that model simulated O₃ mixing ratios
68 within the boundary layer were significantly underestimated during spring-summer, compared
69 with ARCTAS measurements. More recently, Monks et al. (2015) further demonstrated that
70 model simulated O₃ mixing ratios in the Arctic at the surface and in the upper troposphere were
71 generally lower than the observations. In addition, a recent study by Christian et al. (2017)
72 compared O₃ observations from the ARCTAS campaign to GEOS-Chem model simulations and
73 found consistent low biases with the model simulated O₃ at all altitudes except the surface.

74 Field measurements at Summit show that the snowpack emits gas-phase NO_x, PAN, nitrous acid
75 (HONO), as well as hydrogen peroxide (H₂O₂) during spring-summer, when polar sun rises
76 (Ford et al., 2002; Honrath et al., 2002). Although several 1-D models (Thomas et al., 2011,
77 2012; Frey et al., 2013; Murray et al., 2015) have validated the importance of snowpack
78 emissions for surface NO_x as well as O₃ formation, current global chemical transport models
79 (CTMs) usually do not include these emission sources (Zatko et al., 2016).

80 In this study, we examine the abundance and seasonal variations of O₃ and its precursors at
81 Summit with a global chemical transport model, GEOS-Chem CTM, in conjunction with two
82 years of in-situ measurement data for 2008-2010. We first evaluate the model performance in
83 simulating surface O₃ and its precursors, and then implement a series of model updates to resolve
84 the identified model biases. This paper is organized as follows: section 2 describes model
85 methods and observations, followed by detailed comparisons of model simulations against
86 observations for O₃ and O₃ precursors in section 3; conclusions are summarized in section 4.

87 **2. Observational data and model simulations**

88 In situ measurements of NO_x, PAN, and non-methane hydrocarbons (NMHCs) were performed
89 at Summit from July 2008 to June 2010 (Helmig et al., 2014b; Kramer et al., 2015). An
90 automated chemiluminescence instrument was used to measure NO_x (Ridley and Grahek, 1990);
91 a commercial PAN gas chromatography analyzer (PAN-GC, Metcon, In., Boulder, CO) was
92 employed for the measurement of PAN. Measurements of NMHC relied on an automated Gas

93 Chromatography-Flame Ionization Detection (GC-FID) system. Readers are referred to Kramer
94 et al. (2015) and Helmig et al. (2014b) for the details of the measurement techniques and
95 equipment setup. In-situ surface measurements of O₃ at Summit using ultraviolet light absorption
96 technique (Petrovavlovskikh and Oltmans, 2012), and CO data from weekly flask sampling with
97 analysis by a GC/HgO reduction detection instrument (Novellie et al., 2003) and an analyzer
98 based on CO fluorescence in the vacuum ultra violet (Gerbig et al., 1999) were conducted by the
99 National Oceanic and Atmospheric Administration (NOAA), and downloaded from the NOAA
100 Earth System Research Laboratory (ESRL) Global Monitoring Division (GMD) website
101 (<http://www.esrl.noaa.gov/gmd/dv/data/>) for the period between July 2008 and June 2010.
102 Vertical ozonesonde data profiles were also downloaded from NOAA ESRL GMD (McClure-
103 Begley et al., 2014).

104 Simulations of O₃ and related species (NO_x, PAN, NMHCs) were conducted using the GEOS-
105 Chem model (Bey et al., 2001) with coupled O₃-NO_x-VOC-Aerosol chemistry mechanism (i.e.
106 these species interact with each other in the model). The GEOS-Chem CTM is driven by
107 assimilated meteorological data from the Goddard Earth Observing System version 5.2.0
108 (GEOS-5.2.0) of the NASA Global Modeling Assimilation Office. The GEOS-Chem model has
109 been extensively evaluated and applied in a wide range of applications (Martin et al., 2002; Park
110 et al., 2004; Wu et al., 2007; Hudman et al., 2009; Johnson et al., 2010; Huang et al., 2013;
111 Kumar et al., 2013; Zhang et al., 2014; Hickman et al., 2017), including for studies in the Arctic
112 (e.g., Alvarado et al., 2010; Monks et al., 2015; Christian et al., 2017). GEOS-Chem v10-1 with
113 grid resolution of 4° latitude by 5° longitude, and 47 vertical layers was used for the model
114 control simulation. Following McLinden et al. (2000), the Linoz stratospheric O₃ chemistry
115 scheme was used. The simulation was run from June 2007 to June 2010, and the results from the
116 last two years were used in the final analysis. Time series data were archived with 3-hr temporal
117 resolution at the Summit grid box for each model vertical level, including the model bottom
118 layer. For comparison with surface observations at Summit, Greenland, we sampled the data for
119 the model bottom layer. We acknowledge that the topography in GEOS-Chem model is not well
120 resolved at such a coarse model resolution (4° latitude by 5° longitude), and we used the model
121 bottom layer at Summit grid cell for O₃ and its precursors concentrations to compare with
122 surface observations, which worked better than the sampling O₃ and its precursor concentrations
123 at the model vertical layer that is about 3212 m above the sea level (Summit's elevation).

124 Global anthropogenic emissions of NO_x, SO₂, NH₃, and CO in the model were based on the
125 Emission Database for Global Atmospheric Research (EDGAR) v4.2 inventory, which was
126 overwritten by regional emission inventories where applicable, such as the BRAVO inventory
127 for Mexico (Kuhns et al., 2005), the CAC over Canada, the EMEP emissions over Europe, the
128 Model Inter-comparison Study for Asia Phase III (MIX) emissions over Asia (Li et al., 2017),
129 and the US EPA NEI 2011 (NEI11) emission inventory (Simon et al., 2010). The soil NO_x
130 emission scheme followed Hudman et al. (2012). Lightning NO_x emissions were calculated per
131 flash rate based on GEOS-5 computed cloud-top heights (Price and Rind, 1992), which were
132 determined by deep convection and constrained by satellite observations for monthly average
133 flash rates from the Lightning Imaging Sensor and Optical Transient Detector (OTD/LIS)
134 (Sauvage et al., 2007; Murray et al., 2012). Biomass burning emissions were from the Global
135 Fire Emission Database version 4 (GFED4) inventory with monthly resolution (Giglio et al.,
136 2013). The RETRO (Reanalysis of the TROpospheric chemical composition) global
137 anthropogenic NMHC emission inventory (van het Bolscher et al., 2008) was used except for
138 ethane (C₂H₆) and propane (C₃H₈), which followed Xiao et al. (2008, hereafter referred to as
139 X08) for the year 2001. In GEOS-Chem, RETRO used to serve as the default global
140 anthropogenic emission inventory for C₂H₆, however, the annual budget of which has been
141 shown too low compared with observations. Global biofuel emission inventory followed Yevich
142 and Logan (2003), which included emissions for C₂H₆ and C₃H₈. For biogenic VOC emissions,
143 the Model of Emissions of Gases and Aerosols from Nature (MEGAN) scheme (Guenther et al.,
144 2006) was used. Dry deposition of species in GEOS-Chem used a standard resistance-in-series
145 scheme (Wesely, 1989), as implemented in Wang et al. (1998). Wet scavenging followed Liu et
146 al. (2001), including scavenging in convective updraft, rainout (in-cloud) and washout (below-
147 cloud) from convective anvils and large-scale precipitation.

148 We first ran the standard GEOS-Chem model with a-priori emissions and compared the
149 simulation results against observations for various species (including NO_x, PAN, C₂H₆, C₃H₈,
150 CO, and O₃, as shown in Fig. 1). Then we focused on the model-observation discrepancies, and
151 where applicable, made revisions to the model simulations and further evaluated the
152 improvement in model performance, as discussed in details below.

153 **3. Results and Discussions**

154 3.1 NO_x

155 We first combined the two years of data for July 2008 – June 2010 and analyzed their seasonal
156 variations. As shown in Figure 1a, the GEOS-Chem model simulated NO_x agrees well with the
157 observations for July-October. However, compared to observations, the model results
158 significantly overestimate NO_x mixing ratios for November-January by about 150%, while
159 underestimating the data in spring and early summer by approximately 60%. Another challenge
160 for the model simulation is that it does not capture the decrease of NO_x for May - November. We
161 find that during the 2009-2010 winter season, model simulations show several high NO_x spikes
162 with peak NO_x mixing ratios reaching ~ 0.15 ppbv or higher, which is ~ 15 times greater than
163 typical background levels (Fig. 2). These large peaks in NO_x were not observed in the data.
164 Similar peaks were also seen in the model simulations during the 2008-2009 winter season;
165 however, there are no measurements available for this period to compare with.

166 Further analyses showed that the model-simulated high NO_x spikes during wintertime were all
167 associated with transport events from Europe. We carried out a sensitivity study to examine the
168 impacts of European emissions on Arctic NO_x by manually reducing anthropogenic NO_x
169 emissions from the EMEP emission inventory over Europe by 50% (EMEP50). Results showed
170 that surface peak NO_x mixing ratios over Summit during the spike events (e.g., dates around
171 12/09/2009, 12/15/2009, 1/15/2010 and 1/22/2010) from EMEP50 almost declined
172 proportionally by ~ 50% during 2009/12/01-2010/01/31 (Fig. 2), which confirmed that the
173 modeled NO_x spikes at Summit during wintertime were associated with transport from Europe.
174 However, the model simulated NO_x was still significantly higher than observations. Comparisons
175 for surface NO₂ mixing ratios between model simulations and 11 in-situ observational sites over
176 Europe during this period were conducted with data downloaded from <http://ebas.nilu.no>. For
177 detailed site information, NO₂ measurement technique and resolution, refer to Table 1.
178 Measurement data over these two months for each site were averaged to compare with the
179 corresponding grid cell in the model. As shown in Figure 3a, GEOS-Chem overestimated surface
180 NO₂ mixing ratios at these sites by over 66%, compared with observations (slope=1.07;
181 correlation coefficient=0.88).

182 In addition of using EMEP, we carried out another sensitivity study to force anthropogenic NO_x
183 emissions over Europe following EDGAR v4.2 (EURO_EDGAR), with other model
184 configurations identical to control simulations. As shown in Figure 2, the NO_x mixing ratios over
185 Summit during 12/2009-01/2010 agreed much better with observations, especially for January
186 2010, where the model captured the magnitudes of observational peaks. This is because NO_x
187 emissions from EDGAR over Europe (1.97 Tg NO) were 12% lower than those from EMEP
188 (2.24 Tg NO) for the months of 12/2009 and 01/2010. Furthermore, the discrepancy for the
189 differences of surface NO₂ mixing ratios over Europe between EURO_EDGAR and observations
190 was further reduced (by 50%), relative to the control runs, with a model-to-observation slope of
191 0.92 and a correlation coefficient of 0.83 (Fig. 3b). Similarly, we also tested the sensitivity of
192 surface NO_x mixing ratios over Summit in response to the changes in the anthropogenic NO_x
193 emissions from NEI11 over US and MIX over Asia (including Siberia) during these two months,
194 and found that surface NO_x mixing ratios over Summit during these two months were quite close
195 to the control simulations (not shown), reflecting insensitivity to emission perturbations from the
196 US and Asia. Therefore, we conclude that uncertainties in fossil fuel NO_x emissions of EMEP
197 associated with transport events from Europe in the model are the most likely cause for the
198 wintertime NO_x spikes over Summit.

199 For April-July, model simulated monthly mean NO_x mixing ratios over Summit were a factor of
200 two lower than the observations (Fig. 4a). Experiments at Summit by Honrath et al. (1999,
201 2000a, 2000b, 2002) showed upward fluxes of NO_x (2.52×10^8 molecules cm⁻² s⁻¹) from
202 photolysis of nitrate in snowpack during the summertime, leading to enhancement in NO_x levels
203 in the surface layer by approximately 20 pptv, which was comparable to surface NO_x mixing
204 ratios in the Arctic from other sources. Similar results were found over the East Antarctic Plateau
205 snow/ice sheet (Frey et al., 2013; Legrand et al., 2014). The standard GEOS-Chem model did not
206 include the photolysis of nitrate from snowpack, implying a missing source for NO_x in the
207 Arctic/Antarctic boundary layer.

208 In order to test the sensitivity of model simulated surface NO_x mixing ratios to the snowpack
209 emissions, we implemented in the model a constant NO_x flux of $\sim 2.52 \times 10^8$ molecules cm⁻² s⁻¹
210 during April-July over Greenland (60-85° N, 20-60° W), following the measurements conducted
211 at Summit during summertime by Honrath et al. (2002). As a result, we found that on average,

212 the model simulated surface NO_x mixing ratios for April to July over Summit more than doubled
213 that from the control simulation, which improved the agreement between model and observations
214 for April-June (Fig. 4a). However, the assumed NO_x flux from snowpack in the model led to
215 overestimate of NO_x mixing ratios in July and the model was still not able to reproduce the
216 decreasing trend of NO_x for May-October. This decreasing trend of NO_x may be driven by the
217 decreasing NO_x production rate in snowpack resulting from a gradual depletion of the snowpack
218 NO_x reservoir (Van Dam et al., 2015), which is not reflected in the model since we implemented
219 a simple constant NO_x emission flux. Dibb et al. (2007) reported that nitrate concentrations in the
220 Summit snowpack peaked in June and declined toward fall by ~ 1/3. Van Dam et al. (2015)
221 further showed a decreasing trend for NO_x mixing ratios within the snowpack at Summit from
222 June to October. This may partially explain why we would see the declining trend of surface
223 NO_x mixing ratios over Summit from June toward fall. The NO_x emissions from snowpack are
224 affected by a number of factors including nitrate concentrations and solar radiation available and
225 the responses can be very non-linear. Further investigations are needed to account for the
226 seasonal variations of snowpack NO_x emissions from nitrate photolysis in the model, i.e.,
227 constrained by seasonal snowpack NO_x emission flux measurements in the future.

228 **3.2 PAN**

229 We then examined the model performance for PAN, which serves as a reservoir for NO_x. Figure
230 1b shows the comparison of model simulated monthly mean PAN mixing ratios with the
231 measurement data. The model captured the seasonal variation of PAN well, although
232 significantly (by ~ 30%) underestimated the PAN mixing ratios for April-June. By running the
233 model simulation with higher horizontal resolution at 2° latitude by 2.5° longitude (hereafter
234 referred to as GEOS-Chem 2x2.5), we found that the monthly mean PAN mixing ratios over
235 Summit during April-July increased by up to 23.3 pptv compared to the 4x5 simulation (Fig. 4b).
236 This can be explained by two reasons. First, coarse model resolution (e.g., 4x5 horizontal
237 resolution) could artificially smear the intense emission sources throughout the entire grid cell
238 (e.g., over urban regions), leading to underestimates of downwind concentrations for species,
239 e.g., O₃ and O₃ precursors (Jang et al., 1995; Yu et al., 2016). Second, ventilation of the lower
240 atmosphere could be better resolved by a finer model resolution, leading to more efficient
241 vertical advection (Wang et al., 2004; Chen et al., 2009; Yu et al., 2016). However, on average,

242 monthly mean model simulated PAN mixing ratios were still underestimated by 20% during this
243 period, compared with observations. This is consistent with the study by Arnold et al. (2015),
244 which reported that model simulated PAN mixing ratios in GEOS-Chem were lower than
245 ARCTAS observations in the Arctic. Meanwhile, this study also revealed that GEOS-Chem
246 produced less PAN relative to CO in Arctic air parcels that were influenced by fires, compared
247 with other models.

248 Snowpack can emit not only NO_x, but also PAN, based on field studies at Summit during
249 summertime by Ford et al. (2002). GEOS-Chem did not contain snowpack PAN emissions and
250 chemistry. For a sensitivity study, similar to snowpack NO_x emissions as discussed in section
251 3.1, we considered a 24-hr constant flux of 2.52×10^8 molecules cm⁻² s⁻¹ of PAN over Greenland
252 from April to July, following Ford et al. (2002). As a result, model simulated PAN mixing ratios
253 agreed much better with observations (Fig. 4b). Note that there are also other possible reasons
254 that lead to model bias. For instance, a study by Fischer et al. (2014) showed improved
255 agreement between modeled and measured PAN in the high latitudes when assignning a portion
256 of the fire emissions in the model above the boundary layer, and also directly partitioning 40% of
257 NO_x emissions from fires into PAN. We carried out a sensitivity test with similar treatments, but
258 no significant improvements in the model simulated surface PAN were observed at the Summit
259 site. Therefore, we did not include the PAN updates from Fischer et al. (2014) in other model
260 simulations in this study.

261 3.3 NMHC

262 Comparisons of observed surface C₂H₆ and C₃H₈ mixing ratios with GEOS-Chem simulations at
263 Summit are shown in Figures 1c and 1d. The model simulations agreed well with surface
264 measurements of C₃H₈, but systematically overestimated C₂H₆ (by approximately 25% annually),
265 with the largest bias (0.48 ppbv) occurring during summer. This is consistent with the study from
266 Tzompa-Sosa et al., (2017), which used the same model as our study and pointed out that using
267 X08 as global anthropogenic C₂H₆ emission inventory systematically overestimated surface C₂H₆
268 mixing ratios over the Northern Hemisphere, compared with ground-based observations.
269 Anthropogenic C₂H₆ emissions over the US from NEI11 were shown to geographically match
270 the distribution of active oil and natural wells (Tzompa-Sosa et al., 2017), and the most recent

271 MIX has been updated to synergize anthropogenic C₂H₆ emissions from various countries in
272 Asia (Li et al., 2017). Therefore, instead of using global anthropogenic fossil fuel emissions of
273 C₂H₆ following X08, we first conducted sensitivity simulations by overwriting global emission
274 inventories by NEI11 over the US, and MIX over Asia (hereafter referred to as NEI11_MIX).
275 Both NEI11 and MIX contain emissions for the years from 2008 to 2010, which could
276 realistically represent the annual and seasonal variations of C₂H₆ emissions over the US and
277 Asia, thus spatially and temporally better representative of anthropogenic C₂H₆ emissions from
278 mid-latitudes transported to the Arctic regions. In general, model control simulations
279 overestimated annual mean surface C₂H₆ mixing ratios primarily in the Northern Hemisphere,
280 with large differences occurring over Asia and the US by up to 5 ppbv, compared with
281 NEI11_MIX during the period of 07/2008-06/2010 (Fig. S1). All the above changes were driven
282 by the substantial reductions of anthropogenic C₂H₆ emissions between emission inventories,
283 from 3.5 (X08) to 2.5 Tg/yr (MIX) over Asia, and from 1.9 Tg/yr (X08) to 1.4 Tg/yr (NEI11)
284 over the US, reflecting the decreasing trend of anthropogenic C₂H₆ emissions during 2001-2009
285 (Helmig et al., 2014a), because the X08 emission inventory is based on the year 2001.
286 Substantial changes in surface C₂H₆ mixing ratios over the US between control simulations and
287 NEI11_MIX reflected that there existed temporal changes of C₂H₆ emissions from oil and
288 gas productions during the period of 2001-2009. A similar pattern was also found by Tsompa-
289 Sosa et al. (2017). In contrast to the control simulations, NEI11_MIX model simulations showed
290 that monthly mean C₂H₆ mixing ratios over Summit were systematically underestimated by 24%,
291 compared with observations (Fig. 5). Tsompa-Sosa et al. (2017) reported that NEI11 C₂H₆
292 emissions were likely underestimated by 40%, compared with in-situ and aircraft observations
293 over the US. We therefore ran a sensitivity simulation by increasing the NEI11 C₂H₆ emissions
294 by 40% and keeping other model configuration identical to NEI11_MIX (hereafter referred to as
295 NEI11_40_MIX). We found that this update led to an increase in the model simulated annual
296 mean surface C₂H₆ mixing ratios over Summit by only 6% during the period of 07/2008-06/2010
297 (figure not shown), still not able to explain the high model bias.
298 Similar to NEI11_MIX, we further conducted sensitivity studies by only replacing the regional
299 emission inventory for C₂H₆ over the US, with other regions still following X08 (hereafter
300 referred to as NEI11_ONLY). Consequently, model simulated surface C₂H₆ mixing ratios over
301 Summit agreed better with observations during winter-spring (Fig. 5), decreasing the bias from

302 +15% (control simulations) to +6%. However, model simulated C₂H₆ mixing ratios during
303 summer-fall were higher than the observations by over 30%.

304 We then scaled up the MIX emissions for C₂H₆ by 20% over Asia, with other model
305 configurations identical to NEI11_MIX (hereafter referred to as NEI11_MIX20). By doing this,
306 we increased fossil fuel C₂H₆ emissions from 2.5 to 3 Tg/yr. We found that the simulated annual
307 mean surface C₂H₆ mixing ratios at Summit from NEI11_MIX20 agreed quite well with
308 observations (within 1%). Similarly, better agreement between model and observations were
309 found for monthly average values for October - January. However, the new simulation was not
310 able to reproduce the seasonal cycle of C₂H₆ - the model significantly underestimated C₂H₆ in
311 February - April but overestimated it in June - September (Fig. 5). This implies that further
312 assessments of anthropogenic C₂H₆ emissions from MIX over Asia are needed and a more
313 accurate global anthropogenic C₂H₆ emission inventory should be developed and validated to
314 replace X08 in the future. It should be noted that our modeling period reflects a time when there
315 was a reversal of the atmospheric C₂H₆ trend, most likely reflecting emission changes during that
316 time. Atmospheric C₂H₆ had a decreasing trend from 1980 to 2009 (Simpson et al., 2012; Helmig
317 et al., 2014a), but then begun to increase around 2009 (Franco et al., 2015, 2016; Hausmann et
318 al., 2016; Helmig et al., 2016) in the Northern Hemisphere, at a rate of increase that is
319 approximately 4-6 times higher than its earlier rate of decline. It has been argued that the most
320 likely cause for this trend and emissions reversal are increasing emissions from oil and gas
321 production, mostly from North America (Franco et al., 2015, 2016; Hausmann et al., 2016;
322 Helmig et al., 2016). None of the considered inventories consider these emission changes and
323 their timing. Also, note that this standard version of GEOS-Chem does not account for the sink
324 of C₂H₆ from the reaction with chlorine, which could reduce the global annual mean surface
325 C₂H₆ mixing ratios by 0-30%, and the global burden of C₂H₆ by about 20% (Sherwen et al.,
326 2016). This omission likely introduces additional uncertainty for our measurement-model
327 comparison, together with uncertainty in the seasonality of C₂H₆ chemistry.

328 **3.4 CO**

329 Figure 1e shows the comparison of model simulated CO mixing ratios with observations over
330 Summit. Overall, the model generally captures the abundance and seasonal variation of CO.

331 Compared with observations, the annual mean CO mixing ratio was slightly overestimated by
332 about 3 ppbv in the model.

333 **3.5 O₃**

334 Surface O₃ mixing ratios from model simulations and surface observations are compared in
335 Figure 1f. The GEOS-Chem model captured the seasonal variation of O₃ including the spring
336 peak. However, the model shows a systematic low bias for most of the year, in particular for
337 April–July when the surface O₃ mixing ratios were underestimated by ~ 13% (~ 6.5 ppbv). Here
338 we focus our analysis for the possible causes that lead to the model low bias during April–July.

339 As discussed earlier, snowpack emissions due to the photolysis of nitrate in the snow during late
340 spring and summer could contribute to NO_x and HONO levels in the ambient air, which could
341 enhance O₃ production (Crawford et al., 2001; Zhou et al., 2001; Dibb et al., 2002; Honrath et
342 al., 2002; Yang et al., 2002; Grannas et al., 2007; Helmig et al., 2008; Legrand et al., 2014). We
343 ran a sensitivity study to test the response of surface O₃ mixing ratios to the perturbations of NO_x
344 and HONO from snowpack emissions. In addition to snowpack NO_x emissions that are described
345 in Section 3.1, we implemented in the model a constant flux of HONO (4.64×10^7 molecules cm⁻²
346 s⁻¹) from April to July (Honrath et al., 2002). As a result, monthly mean model simulated
347 surface O₃ mixing ratios increased by up to 3 ppbv during this period (Fig. 6). The largest effect
348 occurred in July due to relatively strong solar radiation. O₃ formation due to snowpack emissions
349 in our study was slightly higher than that in Zatzko et al. (2016) because HONO from snowpack
350 emissions was not considered in their study. However, for the months of April and May, surface
351 O₃ mixing ratios only increased by ~ 1 ppbv, compared with the control runs. That is, even after
352 accounting for the snowpack emissions, the model simulated O₃ mixing ratios were still
353 significantly lower than the observations.

354 Comparison of the model simulations at different resolutions (4x5 vs. 2x2.5) showed that the
355 finer resolution simulations substantially increased monthly mean O₃ mixing ratios over Summit
356 by up to 6 ppbv for the months of June and July (Fig. 6). As discussed in section 3.2, fine model
357 resolution can better resolve the emission strengths, which could significantly affect downwind
358 chemical reactions, e.g., O₃ production efficiency (Liang and Jacobson, 2000). Moreover, terrain
359 elevations from fine model resolution are better represented (thus better representative of

360 Summit's elevation), and more efficient vertical ventilation of O₃ and O₃ precursors can be
361 achieved (Wang et al., 2004). Together with the impact of snowpack chemistry, this brought
362 model simulated surface O₃ mixing ratios over Summit to better agreement with observations for
363 June - July. However, there was still a low bias in the model for the months of April and May.

364 Another possible cause for the low O₃ biases in model simulations is the calculated stratosphere-
365 to-troposphere exchange (STE) O₃ flux in the model. Liang et al. (2011) have pointed out that
366 STE could be a significant direct sources of O₃ in the Arctic during spring - summer. We
367 retrieved vertical profiles of O₃ mixing ratios and specific humidity from ozonesondes (0-5 km
368 elevation above the Summit surface) launched at Summit for the months of June and July in
369 2008 and compared those data with model control runs. Ozonesondes were launched intensively
370 during these two months (a total of 19 times). As shown in Figure 7, compared with
371 observations, model simulated O₃ mixing ratios averaged over 0-5 km above ground level were
372 underestimated by 3% and 9% in June and July 2008 (Fig. 7a). However, specific humidity in
373 GEOS-5 was overestimated by 50% and 81% (Fig. 7b) respectively. Ozonesonde data showed
374 that Summit frequently encountered high O₃/low water vapors events (e.g., July 9-11, 2008),
375 which were likely of upper tropospheric/stratospheric origin (Helmig et al., 2007), but these were
376 not captured by the model, which implied that GEOS-Chem possibly underestimated STE for O₃
377 over Summit. This is consistent with the study by Choi et al. (2017), which found low bias with
378 model simulated O₃ mixing ratios for the upper troposphere of the high-latitude Northern
379 Hemisphere, compared with ozonesonde data, and attributed the low bias to an underestimated
380 STE in the model.

381 Misrepresentation of boundary layer height is another factor that could lead to model-data
382 discrepancy in O₃ mixing ratios. The mean springtime afternoon (12:00-14:00, local time)
383 boundary layer height in the model at Summit for the year 2009 was 160 m, which agreed
384 reasonably well with inferred boundary layer heights from vertical balloon soundings (Helmig et
385 al., 2002). Therefore, it is unlikely that model uncertainties in boundary layer height
386 representation in springtime cause the low bias of O₃ mixing ratios between model and
387 observations.

388 **4. Conclusions**

389 We combined model simulations with two-year (July 2008 - June 2010) ground based
390 measurements at Summit, Greenland, to investigate the abundance and seasonal variations of
391 surface O₃ and related species in the Arctic. In general, the GEOS-Chem model was capable of
392 reproducing the seasonal cycles of NO_x, PAN, C₂H₆, C₃H₈, CO, and O₃. However, some major
393 discrepancies between model and observations, especially for NO_x, PAN, C₂H₆, and O₃ were
394 identified.

395 There were significant differences between model simulated NO_x mixing ratios and observations
396 for the spring and winter seasons. The model underestimated NO_x mixing ratios by
397 approximately 50% during late spring to early summer, which was likely due to the missing NO_x
398 emissions from nitrate photolysis in the snowpack. At the same time, the model overestimated
399 NO_x mixing ratios by more than a factor of two in wintertime. Model simulations indicated
400 episodic but frequent transport events from Europe in wintertime leading to NO_x spikes reaching
401 15 times typical NO_x mixing ratios at Summit; these large NO_x spikes were not seen in the
402 observations. We have carried out multiple sensitivity model studies but were still unable to fully
403 reconcile this discrepancy.

404 The model successfully captured the seasonal cycles and the spring maximum PAN mixing
405 ratios, although it underestimated PAN by over 30% during late spring and early summer. Model
406 sensitivity studies revealed that this discrepancy could be largely resolved by accounting for
407 PAN emissions from snowpack.

408 For C₃H₈ and CO, model simulations overall agreed well with the surface measurements.
409 However, the model tended to systematically overestimate surface C₂H₆ mixing ratios by ~ 20%
410 on an annual average, compared with observations. This may be explained by that annual
411 emission budgets of C₂H₆ over US and Asia from X08 emission inventory were higher than
412 those from NEI11 and MIX by over 40%. By replacing X08 over the US with NEI11 for C₂H₆,
413 and scaling up MIX by 20%, the model-observation bias can be resolved, resulting in an annual
414 mean bias of less than 1%. However, care must be taken to interpret this result because we did
415 not take into account other factors that might influence the discrepancy of surface C₂H₆ mixing
416 ratios at Summit between model and observations, such as the C₂H₆ chemistry with chlorine.

417 GEOS-Chem was able to reproduce the seasonal variation of surface O₃ at Summit but
418 persistently underestimated O₃ mixing ratios by ~ 13% (~ 6.5 ppbv) from April to July. This low
419 bias was likely caused by a combination of misrepresentations, including the missing snowpack
420 emissions of NO_x and HONO, inaccurate representation of Summit's elevation with a too coarse
421 model resolution, as well as the underestimated STE.

422 All the results presented above reveal the importance of local snowpack emissions in regulating
423 the atmospheric composition and chemistry over the Arctic. Improvements in global CTMs
424 could likely be achieved by coupling snowpack emissions of reactive gases and photochemistry
425 modules in order to better simulate O₃ precursors and O₃ over snow and ice (Zatko et al., 2016).
426 Moreover, this study also demonstrates that anthropogenic emissions from midlatitudes play an
427 important role in affecting the Arctic atmosphere.

428 **Acknowledgements** This research was funded by U.S. EPA grant 83518901. Findings are solely
429 the responsibility of the grantee and do not necessarily represent the official views of the U.S.
430 EPA. Further, U.S. EPA does not endorse the purchase of any commercial products or services
431 mentioned in the publication. Superior, a high performance computing cluster at Michigan
432 Technological University, was used in obtaining results presented in this publication. L. J.
433 Kramer, D. Helmig and R. E. Honrath thank NASA (grant NNX07AR26G) for supporting the
434 measurements at Summit. S. Wu acknowledges the sabbatical fellowship from the Ocean
435 University of China. D. Helmig acknowledges support from the National Science Foundation,
436 grant NSF AON 1108391. We also thank NOAA ESRL for providing the observational dataset
437 of O₃ and CO. Technical supports from M. Sulprizio and C. Keller are also acknowledged.

438

439 **References**

440 Alvarado, M. J., Logan, J. A., Mao, J., Apel, E., Riemer, D., Blake, D., Cohen, R. C., Min, K.-E.,
441 Perring, A. E., Browne, E. C., Wooldridge, P. J., Diskin, G. S., Sachse, G. W., Fuelberg, H.,
442 Sessions, W. R., Harrigan, D. L., Huey, G., Liao, J., Case-Hanks, A., Jimenez, J. L.,
443 Cubison, M. J., Vay, S. A., Weinheimer, A. J., Knapp, D. J., Montzka, D. D., Flocke, F. M.,

444 Pollack, I. B., Wennberg, P. O., Kurten, A., Crouse, J., St. Clair, J. M., Wisthaler, A.,
445 Mikoviny, T., Yantosca, R. M., Carouge, C. C., and Le Sager, P.: Nitrogen oxides and PAN in
446 plumes from boreal fires during ARCTAS-B and their impact on ozone: an integrated analysis
447 of aircraft and satellite observations, *Atmos. Chem. Phys.*, 10, 9739-9760,
448 doi:10.5194/acp-10-9739-2010, 2010.

449 Arnold, S. R., Emmons, L. K., Monks, S. A., Law, K. S., Ridley, D. A., Turquety, S., Tilmes, S.,
450 Thomas, J. L., Bouarar, I., Flemming, J., Huijnen, V., Mao, J., Duncan, B. N., Steenrod, S.,
451 Yoshida, Y., Langner, J., and Long, Y.: Biomass burning influence on high-latitude
452 tropospheric ozone and reactive nitrogen in summer 2008: a multimodel analysis based on
453 POLMIP simulations, *Atmos. Chem. Phys.*, 15, 6047-6068, doi:10.5194/acp-15-6047-2015,
454 2015.

455 Bey, I., Jacob, D. J., Yantosca, R. M., Logan, J. A., Field, B. D., Fiore, A. M., Li, Q., Liu, H.,
456 Mickley L. J., and Schultz, M. G.: Global modeling of tropospheric chemistry with assimilated
457 meteorology: Model description and evaluation, *J. Geophys. Res.-Atmos.*, 106, 23073-23095,
458 2001.

459 Chen, D., Wang, Y., McElroy, M. B., He, K., Yantosca, R. M., and Le Sager, P.: Regional CO
460 pollution and export in China simulated by the high-resolution nested-grid GEOS-Chem
461 model, *Atmos. Chem. Phys.*, 9, 3825–3839, doi:10.5194/acp-9-3825-2009, 2009.

462 Choi, H., Liu, H., Crawford, J. H., Considine, D. B., Allen, D. J., Duncan, B. N., Horowitz, L.
463 W., Rodriguez, J. M., Strahan, S. E., Zhang, L., Liu, X., Damon, M. R., and Steenrod, S. D.:
464 Global O₃-CO correlations in a chemistry and transport model during July-August: evaluation

465 with TES satellite observations and sensitivity to input meteorological data and emissions,
466 Atmos. Chem. Phys., 17, 8429–8452, doi:10.5194/acp-17-8429-2017, 2017.

467 Christian, K. E., Brune, W. H., and Mao, J.: Global sensitivity analysis of the GEOS-Chem
468 chemical transport model: ozone and hydrogen oxides during ARCTAS (2008), Atmos. Chem.
469 Phys., 17, 3769-3784, doi:10.5194/acp-17-3769-2017, 2017.

470 Crawford, J. H., Davis, D. D., Chen, G., Buhr, M., Oltmans, S., Weller, R., Mauldin, L., Eisele,
471 F., Shetter, R., Lefer, B., Ari- moto, R., and Hogan, A.: Evidence for photochemical produc-
472 tion of ozone at the South Pole surface, Geophys. Res. Lett., 28, 3641–3644, 2001.

473 Dibb, J. E., Arsenault, M., Peterson, M. C., and Honrath, R. E.: Fast nitrogen oxide
474 photochemistry in Summit, Greenland snow, Atmospheric Environment, 36, 2501-2511, 2002.

475 Dibb, J. E., Whitlow, S. I., Arsenault, M.: Seasonal variations in the soluble ion content of snow
476 at Summit, Greenland: Constraints from three years of daily surface snow samples, Atmos.
477 Environ., 41, 5007-5019, doi:10.1016/j.atmosenv.2006.12.010, 2007.

478 Fiore, A. M., Jacob, D. J., Field, B. D., Streets, D. G., Fernandes, S. D., and Jang, C.: Linking
479 ozone pollution and climate change: The case for controlling methane, Geophys. Res. Lett.,
480 29, 1919, doi:10.1029/2002GL015601, 2002.

481 Fischer, E. V., Jacob, D. J., Yantosca, R. M., Sulprizio, M. P., Millet, D. B., Mao, J., Paulot, F.,
482 Singh, H. B., Roiger, A., Ries, L., Talbot, R. W., Dzepina, K., and Pandey Deolal, S.:
483 Atmospheric peroxyacetyl nitrate (PAN): a global budget and source attribution, Atmos.
484 Chem. Phys., 14, 2679-2698, doi:10.5194/acp-14-2679-2014, 2014.

485 Ford, K. M., Shepson, P. B., Bertman, S. B., Honrath, R. E., Peterson, M., Dibb, J. E., and

486 Bottenheim, J. W.: Studies of peroxyacetyl nitrate (PAN) and its interaction with the
487 snowpack at Summit, Greenland, *J. Geophys. Res.*, 107, ACH6, doi:10.1029/2001JD000547,
488 2002.

489 Franco, B., Bader, W., Toon, G., Bray, C., Perrin, A., Fischer, E., Sudo, K., Boone, C., Bovy, B.,
490 Lejeune, B., Servais, C., and Mahieu, E.: Retrieval of ethane from ground-based FTIR solar
491 spectra using improved spectroscopy: Recent burden increase above Jungfraujoch, *J. Quant.*
492 *Spectrosc. Ra.*, 160, 36–49, doi:10.1016/j.jqsrt.2015.03.017, 2015.

493 Franco, B., Mahieu, E., Emmons, L. K., Tzompa-Sosa, Z. A., Fischer, E. V., Sudo, K., Bovy, B.,
494 Conway, S., Griffin, D., Hannigan, J. W., Strong, K., and Walker, K. A.: Evaluating ethane
495 and methane emissions associated with the development of oil and natural gas extraction in
496 North America, *Environ. Res. Lett.*, 11, doi:10.1088/1748-9326/11/4/044010, 2016.

497 Frey, M. M., Brough, N., France, J. L., Anderson, P. S., Traulle, O., King, M. D., Jones, A. E.,
498 Wolff, E. W., and Savarino, J.: The diurnal variability of atmospheric nitrogen oxides (NO and
499 NO₂) above the Antarctic Plateau driven by atmospheric stability and snow emissions, *Atmos.*
500 *Chem. Phys.*, 13, 3045-3042, doi:10.5194/acp-13-3045-2013, 2013.

501 Gerbig, C., Schmitgen, S., Kley, D., Volz-Thomas, A., Dewey, K., and Haaks, D.: An improved
502 fast-response vacuum-UV resonance fluorescence CO instrument, *J. Geophys. Res.*, 104, D1,
503 1699-1704, 1999.

504 Giglio, L., Randerson, J. T., and van der Werf, G. R.: Analysis of daily, monthly, and annual
505 burned area using the fourth-generation global fire emissions database (GFED4), *J. Geophys.*
506 *Res. Biogeosci.*, 118, 1, 317-328, doi:10.1002/jgrg.20042, 2013.

507 Grannas, A. M., Jones, A. E., Dibb, J., Ammann, M., Anastasio, C., Beine, H. J., Bergin, M.,
508 Bottenheim, J., Boxe, C. S., Carver, G., Chen, G., Crawford, J. H., Domine, F., Frey, M. M.,
509 Guzman, M. I., Heard, D. E., Helmig, D., Hoffmann, M.R., Honrath, R. E., Huey, L. G.,
510 Hutterli, M., Jacobi, H. W., Klán, P., Lefer, B., McConnell, J., Plane, J., Sander, R., Savarino,
511 J., Shepson, P. B., Simpson, W. R., Sodeau, J. R., von Glasow, R., Weller, R., Wolff, E. W.,
512 and Zhu, T.: An overview of snow photochemistry: evidence, mechanisms and impacts,
513 *Atmos. Chem. Phys.*, 7, 4329–4373, doi:10.5194/acp-7-4329-2007, 2007.

514 Guenther, A., Karl, T., Harley, P., Wiedinmyer, C., Palmer, P. I., and Geron C.: Estimate of
515 global terrestrial isoprene emissions using MEGAN (Model of Emissions of Gases and
516 Aerosols from Nature), *Atmos. Chem. Phys.*, 6, 3181-3210, doi:10.5194/acp-6-3181-2006,
517 2006.

518 Hausmann, P., Sussmann, R., and Smale, D.: Contribution of oil and natural gas production to
519 renewed increase in atmospheric methane (2007–2014): top–down estimate from ethane and
520 methane column observations, *Atmos. Chem. Phys.*, 16, 3227–3244, doi:10.5194/acp-16-
521 3227-2016, 2016.

522 Helmig, D., Boulter, J., David, D., Birks, J. W., Cullen, N. J., Steffen, K., Johnson, B. J. and
523 Oltmans, S. J.: Ozone and meteorological boundary-layer conditions at Summit, Greenland,
524 during 3-21 June 2000, *Atmos. Environ.*, 36(15–16), 2595–2608, doi:10.1016/S1352-
525 2310(02)00129-2, 2002.

526 Helmig, D., Oltmans, S. J., Morse, T. O., and Dibb, J. E.: What is causing high ozone at Summit,
527 Greenland?, *Atmos. Environ.*, 41, 5031-5043, doi:10.1016/j.atmosenv.2006.05.084, 2007.

528 Helmig, D., Johnson, B., Oltmans, S. J., Neff, W., Eisele, F., and Davis, D. D.: Elevated ozone in
529 the boundary-layer at South Pole, *Atmos. Environ.*, 42, 2788–2803, 2008.

530 Helmig, D., Petrenko, V., Martinerie, P., Witrant, E., Röckmann, T., Zuiderweg, A., Holzinger,
531 R., Hueber, J., Thompson, C., White, J. W. C., Sturges, W., Baker, A., Blunier, T., Etheridge,
532 D., Rubino, M., and Tans, P.: Reconstruction of Northern Hemisphere 1950–2010
533 atmospheric non-methane hydrocarbons, *Atmos. Chem. Phys.*, 14, 1463–1483,
534 doi:10.5194/acp-14-1463-2014, 2014a.

535 Helmig, D., Stephens, C., Caramore, J., and Hueber, J.: Seasonal behavior of non-methane
536 hydrocarbons in the firm air at Summit, Greenland, *Atmos. Environ.*, 85, 234-246,
537 doi:10.1016/j.atmosenv.2013.11.021, 2014b.

538 Helmig, D., Rossabi, S., Hueber, J., Tans, P., Montzka, S. A., Masarie, K., Thoning, K., Plass-
539 Duelmer, C., Claude, A., Carpenter, L. J., Lewis, A. C., Punjabi, S., Reimann, S., Vollmer,
540 M. K., Steinbrecher, R., Hannigan, J. W., Emmons, L. K., Mahieu, E., Franco, B., Smale, D.,
541 and Pozzer, A.: Reversal of global atmospheric ethane and propane trends largely due to US
542 oil and natural gas production, *Nat. Geosci.*, 9, 490–495, doi:10.1038/ngeo2721, 2016.

543 Hickman, J. E., Huang, Y., Wu, S., Diru, W., Groffman, P. M., Tully, K. L., and Palm, C. A.:
544 Nonlinear response of nitric oxide fluxes to fertilizer inputs and the impacts of agricultural
545 intensification on tropospheric ozone pollution in Kenya, *Glob. Change Biol.*, 23, 3193-3204,
546 doi:10.1111/gcb.13644, 2017.

547 Hollaway, M. J., Arnold, S. R., Challinor, A. J., and Emberson, L. D.: Intercontinental trans-
548 boundary contributions to ozone-induced crop yield losses in the North Hemisphere,

549 Biogeosciences, 9, 271-292, doi: 10.5194/bg-9-271-2012, 2012.

550 Honrath, R. E., Peterson, M. C., Guo, S., Dibb, J. E., Shepson, P. B., and Campbell, B.: Evidence
551 of NO_x production within or upon ice particles in the Greenland snowpack, *Geophys. Res.*
552 *Lett.*, 26, 695-698, 1999.

553 Honrath, R. E., Guo, S., Peterson, M. C., Dziobak, M. P., Dibb, J. E., and Arsenault, M. A.:
554 Photochemical production of gas phase NO_x from ice crystal NO₃⁻, *J. Geophys. Res.*, 105,
555 24183–24190, 2000a.

556 Honrath, R. E., Peterson, M. C., Dziobak, M. P., Dibb, J. E., Arsenault, M. A., and Green, S. A.:
557 Release of NO_x from Sunlight-irradiated Midlatitude Snow, *Geophys. Res. Lett.*, 27, 2237–
558 2240, 2000b.

559 Honrath, R. E., Lu, Y., Peterson, M. C., Dibb, J. E., Arsenault, M. A., Cullen, N. J., and Steffen,
560 K.: Vertical fluxes of NO_x, HONO, and HNO₃ above the snowpack at Summit, Greenland,
561 *Atmos. Environ.*, 36, 2629-2640, doi:10.1016/S1352-2310(02)00132-2, 2002.

562 Huang, Y., Wu, S., Dubey, M. K., and French, N. H. F.: Impact of aging mechanism on model
563 simulated carbonaceous aerosols, *Atmos. Chem. Phys.*, 13, 6329–6343, doi:10.5194/acp-13-
564 6329-2013, 2013.

565 Hudman, R. C., Moore, N. E., Mebust, A. K., Martin, R. V., Russell, A. R., Valin, L. C., and
566 Cohen, R. C.: Steps towards a mechanistic model of global soil nitric oxide emissions:
567 implementation and space based-constraints, *Atmos. Chem. Phys.*, 12, 7779-7795, doi:
568 10.5194/acp-12-7779- 2012, 2012.

569 Hudman, R. C., Murray, L. T., Jacob, D. J., Turquety, S., Wu, S., Millet, D. B., Avery, M.,
570 Goldstein, A. H., and Holloway, J.: North American influence on tropospheric ozone and the
571 effects of recent emission reductions: Constraints from ICARTT observations, *J. Geophys.*

572 Res., 114, D07302, doi:10.1029/2008JD010126, 2009.

573 Jacob, D. J., Wofsy, S. C., Bakwin, P. S., Fan, S.-M., Harriss, R. C., Talbot, R. W., Bradshaw, J.
574 D., Sandholm, S. T., Singh, H. B., Browell, E. V., Gregory, G. L., Sachse, G. W., Shipham,
575 M. C., Blake, D. R., and Fitzjarrald, D. R.: Summertime photochemistry of the troposphere at
576 high northern latitudes, *J. Geophys. Res.*, 97, D15, 16421-16431, doi:10.1029/91JD01968,
577 1992.

578 Jang, J.-C., Jeffries, H., Byun, D., and Pleim, J.: Sensitivity of ozone to model grid resolution – I.
579 Application of high resolution regional acid deposition model, *Atmos. Environ.*, 29, 3085-
580 3100, doi:10.1016/1352-2310(95)00118-I, 1995.

581 Johnson, M.S., Meskhidze, N., Solmon, F., Gasso, S., Chuang, P. Y., Gaiero, D. M., Yantosca,
582 R. M., Wu, S., Wang, X., Carouge, C.: Modeling Dust and Soluble Iron Deposition to the
583 South Atlantic Ocean, *J. Geophys. Res.*, 115, D15202, doi:10.1029/2009JD013311, 2010.

584 Kramer, L. J., Helmig, D., Burkhardt, J. F., Stohl, A., Oltmans, S., and Honrath, R. E.: Seasonal
585 variability of atmospheric nitrogen oxides and non-methane hydrocarbons at the GEOSummit
586 station, Greenland, *Atmos. Chem. Phys.*, 15, 6827-6849, doi:10.5194/acp-15-6827-2015,
587 2015.

588 Kuhns, H., Knipping, E. M., and Vukovich, J. M.: Development of a United States-Mexico emis-
589 sions inventory for the Big Bend Regional Aerosol and Visibility Observational (BRAVO)
590 Study, *JAPCA J. Air Waste M.*, 55, 677–692, 2005.

591 Kumar, A., Wu, S., Weise, M. F., Honrath, R., Owen, R. C., Helmig, D., Kramer, L., Val Martin,
592 M., and Li, Q.: Free-troposphere ozone and carbon monoxide over the North Atlantic for

593 2001–2011, *Atmos. Chem. Phys.*, 13, 12537–12547, doi:10.5194/acp-13-12537-2013, 2013.

594 Legrand, M., Preunkert, S., Frey, M., Bartels-Rausch, Th., Kukui, A., King, M. D., Savarino, J.,
595 Kerbrat, M., and Jourdain, B.: Large mixing ratios of atmospheric nitrous acid (HONO) at
596 Concordia (East Antarctic Plateau) in summer: a strong source from surface snow?, *Atmos.*
597 *Chem. Phys.*, 14, 9963–9976, doi:10.5194/acp-14-9963-2014, 2014.

598 Li, M., Zhang, Q., Kurokawa, J., Woo, J. H., He, K. B., Lu, Z., Ohara, T., Song, Y., Streets, D.
599 G., Carmichael, G. R., Cheng, Y. F., Hong, C. P., Huo, H., Jiang, X. J., Kang, S. C., Liu, F.,
600 Su, H., and Zheng, B.: MIX: a mosaic Asian anthropogenic emission inventory under the
601 international collaboration framework of the MICS-Asia and the HTAP, *Atmos. Chem. Phys.*,
602 17, 935–963, doi:10.5194/acpd-17-935-2017.

603 Liang, J., and Jacobson, M. Z.: Effects of subgrid segregation on ozone production efficiency in
604 a chemical model, *Atmos. Environ.*, 34, 2975–2982, doi:10.1016/S1352-2310(99)00520-8,
605 2000.

606 Liang, Q., Rodriguez, J. M., Douglass, A. R., Crawford, J. H., Olson, J. R., Apel, E., Bian, H.,
607 Blake, D. R., Brune, W., Chin, M., Colarco, P. R., da Silva, A., Diskin, G. S., Duncan, B. N.,
608 Huey, L. G., Knapp, D. J., Montzka, D. D., Nielsen, J. E., Pawson, S., Riemer, D. D.,
609 Weinheimer, A. J., and Wisthaler, A.: Reactive nitrogen, ozone and ozone production in the
610 Arctic troposphere and the impact of stratosphere-troposphere exchange, *Atmos. Chem. Phys.*,
611 11, 13181–13199, doi:10.5194/acp-11-13181-2011, 2011.

612 Liu, H. Y., Jacob, D. J., Bey, I., and Yantosca, R. M.: Constraints from pb-210 and Be-7 on wet
613 deposition and transport in a global three-dimensional chemical tracer model driven by

614 assimilated meteorological fields, *J. Geophys. Res.-Atmos.*, 106, 12109-12128, doi:
615 10.1029/2000JD900839, 2001.

616 Martin, R. V., Jacob, D. J., Logan, J. A., Bey, I., Yantosca, R. M., Staudt, A. C., Li, Q., Fiore, A.
617 M., Duncan, B. N., and Liu, H.: Interpretation of TOMS observations of tropical tropospheric
618 ozone with a global model and in situ observations, *J. Geophys. Res.*, 107(D18), ACH 4-1-
619 ACH 4-27, doi: 10.1029/2001JD001480, 2002.

620 McClure-Begley, A., Petropavlovskikh, I., Oltmans, S.: NOAA Global Monitoring Surface
621 Ozone Network. 1973-2014. National Oceanic and Atmospheric Administration, Earth
622 Systems Research Laboratory Global Monitoring Division. Boulder, CO. DATE ACCESSED:
623 4/23/2017, <http://dx.doi.org/10.7289/V57P8WBF>, 2014.

624 McLinden, C. A., Olsen, S. C., Hannegan, B., Wild, O., Prather, M. J., and Sundet, J.:
625 Stratospheric ozone in 3-D models: A simple chemistry and the cross-tropopause flux, *J.*
626 *Geophys. Res.*, 105, D11, 14653-14665, doi:10.1029/2000JD900124, 2000.

627 Monks, S. A., Arnold, S. R., Emmons, L. K., Law, K. S., Turquety, S., Duncan, B. N.,
628 Flemming, J., Huijnen, V., Tilmes, S., Langner, J., Mao, J., Long, Y., Thomas, J. L., Steenrod,
629 S. D., Raut, J. C., Wilson, C., Chipperfield, M. P., Diskin, G. S., Weinheimer, A., Schlager,
630 H., and Ancellet, G.: Multi-model study of chemical and physical controls on transport of
631 anthropogenic and biomass burning pollution to the Arctic, *Atmos. Chem. Phys.*, 15, 3575-
632 3603, doi:10.5194/acp-15-3575-2015, 2015.

633 Murray, K. A., Kramer, L. J., Doskey, P. V., Ganzeveld, L., Seok, B., Van Dam, B., and Helmig,
634 D.: Dynamics of ozone and nitrogen oxides at Summit, Greenland. II. Simulating snowpack

635 chemistry during a spring high ozone event with a 1-D process-scale model, *Atmos. Environ.*,
636 117, 110–123, doi:10.1016/j.atmosenv.2015.07.004, 2015.

637 Murray, L. T., Jacob, D. J., Logan, J. A., Hudman, R. C., and Koshak, W. J.: Optimized regional
638 and interannual variability of lightning in a global chemical transport constrained by LIS/OTD
639 satellite data, *J. Geophys. Res.*, 117, D20307, doi:10.1029/2012JD017934, 2012.

640 Novelli, P.C., Masarie, K. A., Lang, P. M., Hall, B. D., Myers, R. C., and Elkins, J. W.: Re-
641 analysis of tropospheric CO trends: Effects of the 1997-1998 wild fires, *J. Geophys. Res.*, 108,
642 D15, 4464, doi:10.1029/2002JD003031, 2003.

643 Park, R. J., Jacob, D. J., Field, B. D., Yantosca, R. M., and Chin, M.: Natural and transboundary
644 pollution influences on sulfate-nitrate-ammonium aerosols in the United States: Implications
645 for policy, *J. Geophys. Res.-Atmos.*, 109, D15204, doi:10.1029/2003JD004473, 2004.

646 Petropavlovskikh, I. and Oltmans, S. J.: Tropospheric Ozone Measurements, 1973-2011,
647 Version: 2012-07-10, NOAA, available at: <ftp://aftp.cmdl.noaa.gov/data/ozwv/SurfaceOzone/>,
648 2012.

649 Price, C. and Rind, D.: A simple lightning parameterization for calculating global lightning
650 distributions, *J. Geophys. Res.*, 97, 9919-9933, doi:10.1029/92JD00719, 1992.

651 Ridley, B. A., and Grahek, F.: A small, low flow, high sensitivity reaction vessel for NO
652 chemiluminescence detectors, *Am. Meteorol. Soc.*, 7, 307-311, 1990.

653 Sauvage, B., Martin, R. V., van Donkelaar, A., Liu, X., Chance, K., Jaeglé, L., Palmer, P. I., Wu,
654 S., and Fu, T.-M.: Remote sensed and in situ constraints on processes affecting tropical tropo-
655 spheric ozone, *Atmos. Chem. Phys.*, 7, 815–838, doi:10.5194/acp-7-815-2007, 2007.

656 Sherwen, T., Schmidt, J. A., Evans, M. J., Carpenter, L. J., Großmann, K., Eastham, S. D.,
657 Jacob, D. J., Dix, B., Koenig, T. K., Sinreich, R., Ortega, I., Volkamer, R., Saiz-Lopez, A.,
658 Prados-Roman, C., Mahajan, A. S., and Ordóñez, C.: Global impacts of tropospheric halogens
659 (Cl, Br, I) on oxidants and composition in GEOS-Chem, *Atmos. Chem. Phys.*, 16, 12239–
660 12271, doi:10.5194/acp-16-12239-2016, 2016.

661 Shindell, D. T., Chin, M., Dentener, F., Doherty, R. M., Faluvegi, G., Fiore, A. M., Hess, P.,
662 Koch, D. M., MacKenzie, I. A., Sanderson, M. G., Schultz, M., Stevenson, D. S., Teich, H.,
663 Textor, C., Wild, O., Bergmann, D. J., Bey, I., Bian, H., Cuvelier, C., Duncan, B. N., Folberth,
664 G., Horowitz, L. W., Jonson, J., Kaminski, J. W., Marmer, E., Park, R., Pringle, K. J.,
665 Schroeder, S., Szopa, S., Takemura, T., Zeng, G., Keating, T. J., and Zuber, A.: A multi-model
666 assessment of pollution transport to the Arctic, *Atmos. Chem. Phys.*, 8, 5353-5372,
667 doi:10.5194/acp-8-5353-2008, 2008.

668 Simon, H., Beck, L., Bhave, P. V., Divita, F., Hsu, Y., Luecken, D., Mobley, J. D., Pouliot, G.
669 A., Reff, A., Sarwar, G., and Strum, M.: The development and uses of EPA's SPECIATE
670 database, *Atmospheric Pollution Research*, 196-206, 10.5094/apr.2010.026, 2010.

671 Simpson, I. J., Sulbaek Andersen, M. P., Meinardi, S., Bruhwiler, L., Blake, N. J., Helmig, D.,
672 Rowland, F. S. and Blake, D. R.: Long-term decline of global atmospheric ethane
673 concentrations and implications for methane, *Nature*, 488(7412), 490–494,
674 doi:10.1038/nature11342, 2012.

675 Thomas, J. L., Stutz, J., Lefer, B., Huey, L. G., Toyota, K., Dibb, J. E., and von Glasow, R.:
676 Modeling chemistry in and above snow at Summit, Greenland – Part 1: Model description and

677 results, *Atmos. Chem. Phys.*, 11, 4899–4914, doi:10.5194/acp-11-4899-2011, 2011.

678 Thomas, J. L., Dibb, J. E., Huey, L. G., Liao, J., Tanner, D., Lefer, B., von Glasow, R., and
679 Stutz, J.: Modeling chemistry in and above snow at Summit, Greenland – Part 2: Impact of
680 snowpack chemistry on the oxidation capacity of the boundary layer, *Atmos. Chem. Phys.*, 12,
681 6537–6554, doi:10.5194/acp-12-6537-2012, 2012.

682 Tzompa-Sosa, Z. A., Mahieu, E., Franco, B., Keller, C. A., Turner, A. J., Helmig, D., Fried, A.,
683 Richter, D., Weibring, P., Walega, J., Yacovitch, T. I., Herndon, S. C., Blake, D. R., Hase, F.,
684 Hannigan, J. W., Conway, S., Strong, K., Schneider, M., and Fischer, E. V.: Revisiting global
685 fossil fuel and biofuel emissions of ethane, *J. Geophys. Res. Atmos.*, 122,
686 doi:10.1002/2016JD025767, 2017.

687 Unger, N., Shindell, D. T., Koch, D. M., and Streets, D. G.: Cross influences of ozone and
688 sulfate precursor emissions changes on air quality and climate, *Proc. Natl. Acad. Sci.*, 103,
689 4377-4380, doi:10.1073/pnas.0508769103, 2006.

690 van het Bolscher, M., Pereira, J., Spesso, A., Dalsoren, S., van Noije, T., and Szopa, S.:
691 REanalysis of the TROpospheric chemical composition over the past 40 years: A long-term
692 global modeling study of tropospheric chemistry, Max Plank Inst. For Meteorology, Hamburg,
693 Germany, 77, 2008.

694 Van Dam, B., Helmig, D., Toro, C., Doskey, P., Kramer, L., Murray, K., Ganzeveld, L., and
695 Seok, B.: Dynamics of ozone and nitrogen oxides at Summit, Greenland: I. Multi-year
696 observations in the snowpack, *Atmos. Environ.*, 123, 268-284,
697 doi:10.1016/j.atmosenv.2015.09.060, 2015.

698 Walker, T. W., Jones, D. B. A., Parrington, M., Henze, D. K., Murray, L. T., Bottenheim, J. W.,
699 Anlauf, K., Worden, J. R., Bowman, K. W., Shim, C., Singh, K., Kopacz, M., Tarasick, D. W.,
700 Davies, J., von der Gathen, P., Thompson, A. M., and Carouge, C. C.: Impacts of midlatitude
701 precursor emissions and local photochemistry on ozone abundances in the Arctic, *J. Geophys.*
702 *Res.*, 117, D01305, doi:10.1029/2011JD016370, 2012.

703 Wang, Y. H., Jacob, D. J., and Logan, J. A.: Global simulation of tropospheric O₃-NO_x-hydro-
704 carbon chemistry 1. Model formulation, *J. Geophys. Res.-Atmos.*, 103, 10713-10725, doi:
705 10.1029/98JD00158, 1998.

706 Wang, Y. X., McElroy, M. B., Jacob, D. J., and Yantosca, R. M.: A nested grid formulation for
707 chemical transport over Asia: Applications to CO, *J. Geophys. Res.*, 109, D22307,
708 doi:10.1029/2004JD005237, 2004.

709 Wesely, M. L.: Parameterization of surface resistances to gaseous dry deposition in regional-
710 scale numerical-models, *Atmos. Environ.*, 23, 1293-1304, doi:10.1016/0004-6981(89)90153-
711 4, 1989.

712 Wespes, C., Emmons, L., Edwards, D. P., Hannigan, J., Hurtmans, D., Saunio, M., Coheur, P.-
713 F., Clerbaux, C., Coffey, M. T., Batchelor, R. L., Lindenmaier, R., Strong, K., Weinheimer, A.
714 J., Nowak, J. B., Ryerson, T. B., Crouse, J. D., and Wennberg, P. O.: Analysis of ozone and
715 nitric acid in spring and summer Arctic pollution using aircraft, ground-based, satellite
716 observations and MOZART-4 model: source attribution and partitioning, *Atmos. Chem. Phys.*,
717 12, 237–259, doi:10.5194/acp-12-237-2012, 2012.

718 Wu, S., Mickley, L. J., Jacob, D. J., Logan, J. A., Yantosca, R. M., and Rind, D.: Why are there

719 large differences between models in global budgets of tropospheric ozone?, *J. Geophys. Res.*,
720 112(D5), D05302, doi:10.1029/02006JD007801, 2007.

721 Xiao, Y., Logan, J. A., Jacob, D. J., Hudman, R. C., Yantosca, R., and Blake, D. R.: The global
722 budget of ethane and regional constraints on U.S. sources, *J. Geophys. Res.*, 113, D21306,
723 doi:10.1029/2007JD009415, 2008.

724 Yang, J., Honrath, R. E., Peterson, M. C., Dibb, J. E., Sumner, A. L., Shepson, P. B., Frey, M.,
725 Jacobi, H.-W., Swanson, A., and Blake, N.: Impacts of snowpack emissions on deduced levels
726 of OH and peroxy radicals at Summit, Greenland, *Atmos. Environ.*, 36, 2523-2534,
727 doi:10.1016/S1352-2310(02)00128-0, 2002.

728 Yevich, R., and Logan, J. A.: An assessment of biofuel use and burning of agricultural waste in
729 the developing world, *Global Biogeochem. Cy.*, 17, 1095, doi:10.1029/2002GB001952, 2003.

730 Yu, K., Jacob, D. J., Fisher, J. A., Kim, P. S., Marais, E. A., Miller, C. C., Travis, K. R., Zhu, L.,
731 Yantosca, R. M., Sulprizio, M. P., Cohen, R. C., Dibb, J. E., Fried, A., Mikoviny, T., Ryerson,
732 T. B., Wennberg, P. O., and Wisthaler, A.: Sensitivity to grid resolution in the ability of a
733 chemical transport model to simulate observed oxidant chemistry under high-isoprene
734 conditions, *Atmos. Chem. Phys.*, 16, 4369–4378, doi:10.5194/acp-16-4369-2016, 2016.

735 Zatzko, M. C., Geng, L., Alexander, B., Sofen, E. D., and Klein, K.: The impact of snow nitrate
736 photolysis on boundary layer chemistry and the recycling and redistribution of reactive
737 nitrogen across Antarctica and Greenland in a global chemical transport model, *Atmos. Chem.*
738 *Phys.*, 16, 2819-2842, doi:10.5194/acpd-16-2819-2016, 2016.

739 Zhang, H., Wu, S., Huang, Y., and Wang, Y.: Effects of stratospheric ozone recovery on

740 photochemistry and ozone air quality in the troposphere, *Atmos. Chem. Phys.*, 14, 4079-4086,
741 doi:10.5194/acp-14-4079-2014, 2014.

742 Zhou, X., Beine, H. J., Honrath, R. E., Fuentes, J., Simpson, W., Shepson, P. B., and Bottenheim,
743 J. W.: snowpack photochemical production of HONO: a major source of OH in the Arctic
744 boundary layer in springtime, *Geophys. Res. Lett.*, 28, 21, 4087-4090, 2001.

745

746

747

748

749

750

751

752

753

754

755

756

757

758

759

760

761

762

763

764

765

766

767 **Table 1.** Surface NO₂ measurements over Europe during 2009/12/01-2010/01/31.

Site ID	Site name	Lat. (°N)	Lon. (°E)	Altitude a.s.l (m)	Technique	Resolution
BE0001R	Offagne	49.88	5.20	430	chemiluminescence	hourly
BE0032R	Eupen	50.63	6.00	295	chemiluminescence	hourly
DE0001R	Westerland	54.93	8.31	12	NaJ_solution	daily
DK0008R	Anholt	56.72	11.52	40	UV_fluorescence	hourly
FI0096G	Pallas	67.97	24.12	340	chemiluminescence	hourly
GB0014R	High Muffles	54.33	-0.80	267	chemiluminescence	daily
NL0009R	Kollumerwaard	53.33	6.28	1	chemiluminescence	hourly
NO0001R	Birkenes	58.38	8.25	190	glass sinter	daily
NO0039R	Kårvatn	62.78	8.88	210	glass sinter	daily
NO0056R	Hurdal	60.37	11.08	300	glass sinter	daily
SE0005R	Bredkålen	63.85	15.3	404	abs_tube	daily

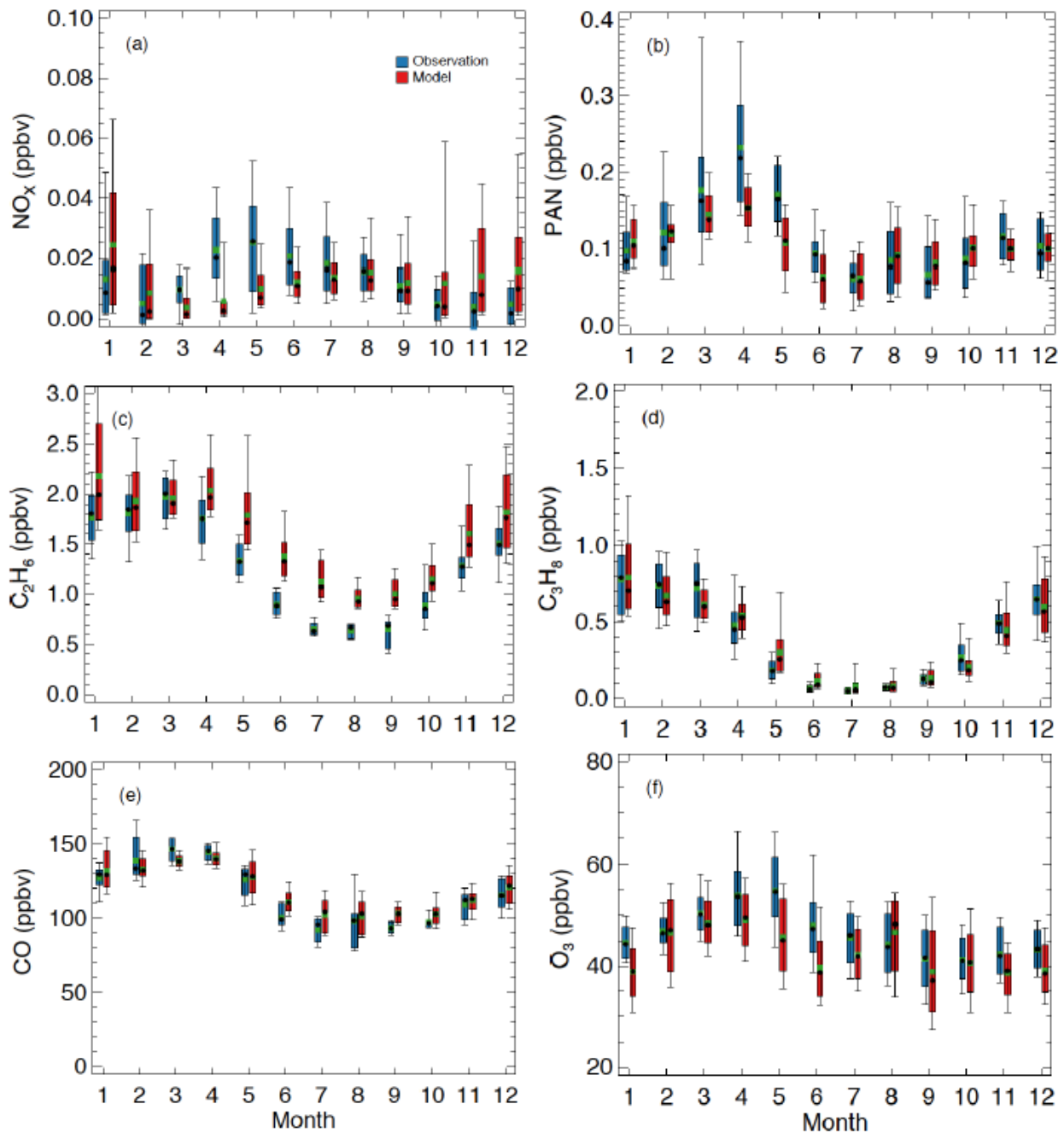
768

769

770

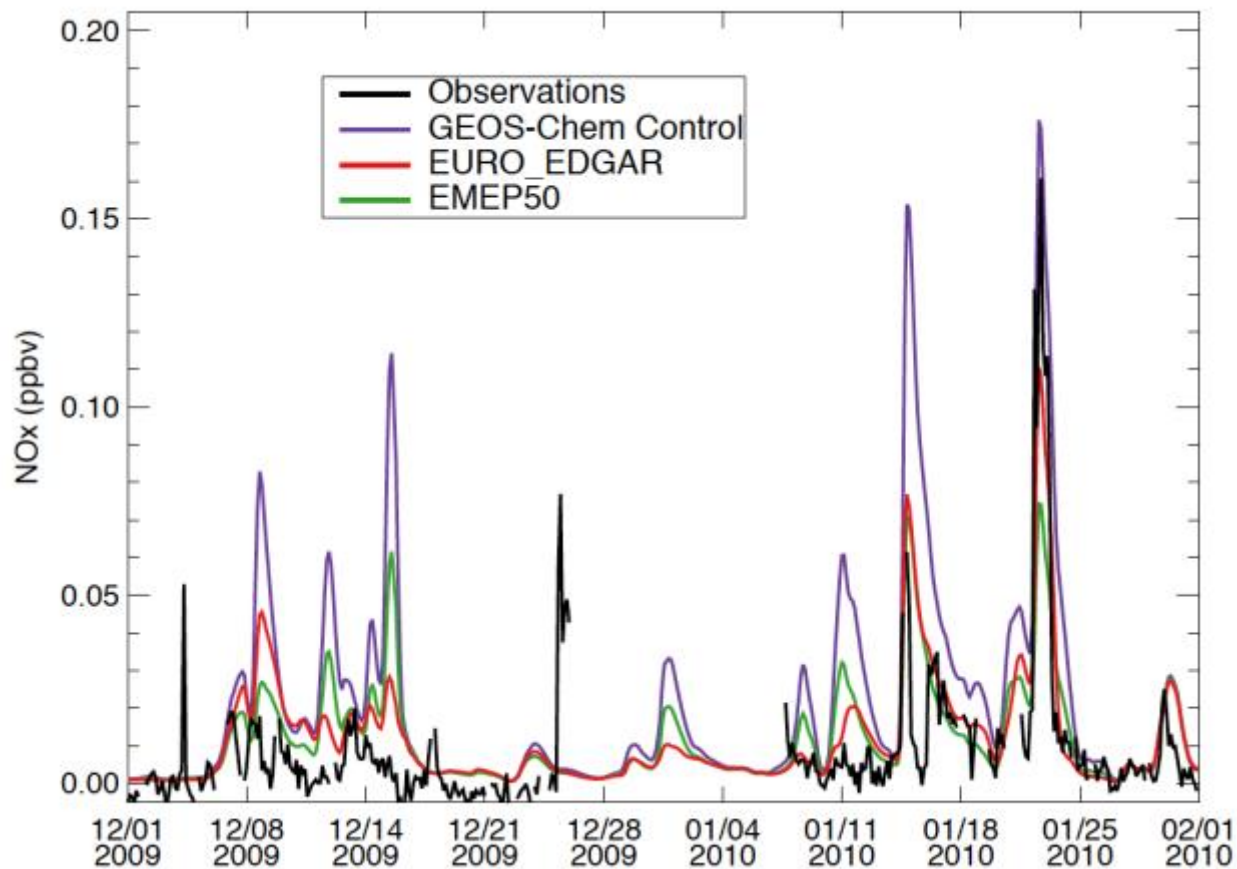
771

772



773

774 **Figure 1.** Box plot comparison for seasonal variations of (a) NO_x , (b) PAN, (c) C_2H_6 , (d) C_3H_8 ,
 775 (e) CO, and (f) O_3 between GEOS-Chem model simulations (red) and measurements (blue) at
 776 Summit for the period of 2008/07-2010/06. Data shown are monthly averages during this period.
 777 The thick (thin) bars represent the 67% (95%) confidence intervals. Black and green dots
 778 represent median and mean values, respectively. The statistics are based on daily averages.



779

780 **Figure 2.** Timeseries of surface NO_x mixing ratios over Summit from observations, GEOS-
 781 Chem model control simulations, EURO_EDGAR, and EMEP50 during 2009/12/01-2010/01/31.
 782 EURO_EDGAR represents simulations with anthropogenic NO_x emissions over Europe
 783 following EDGAR v4.2, while EMEP50 denotes simulations with anthropogenic NO_x emissions
 784 from the EMEP emission inventory over Europe reduced by 50%, with other model
 785 configurations identical to the control simulations.

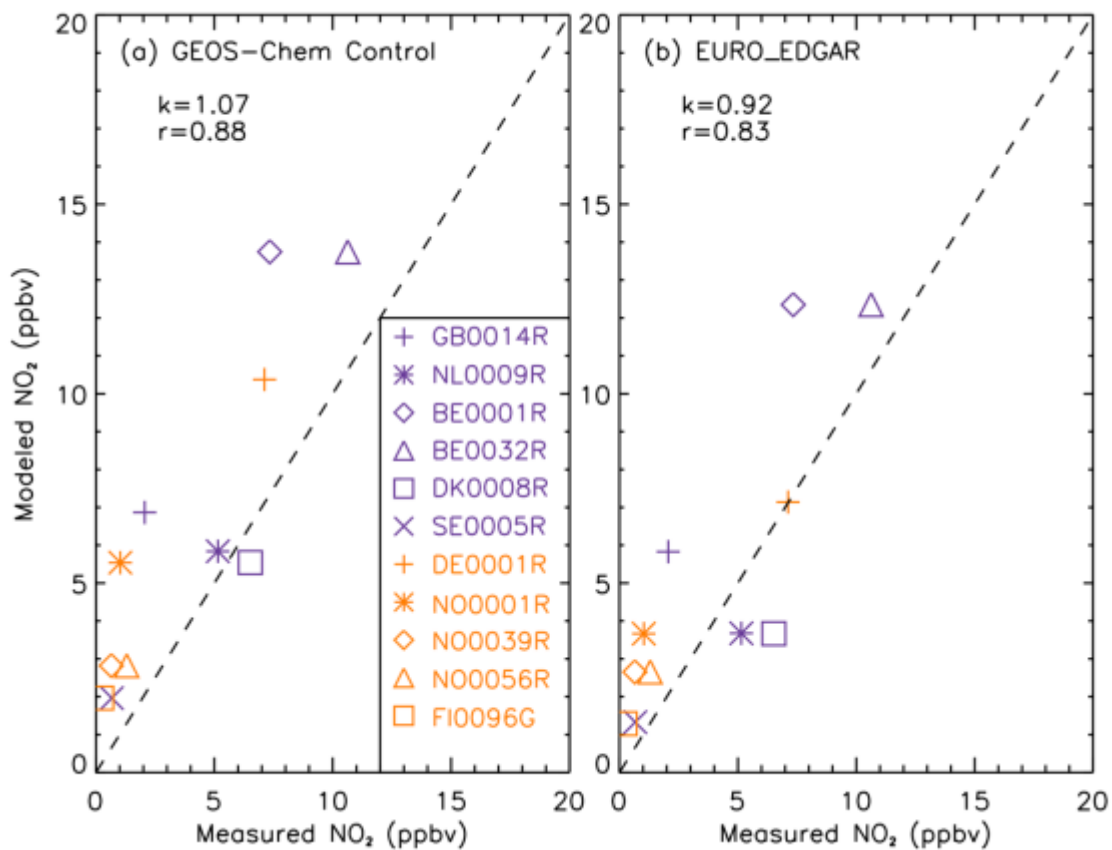
786

787

788

789

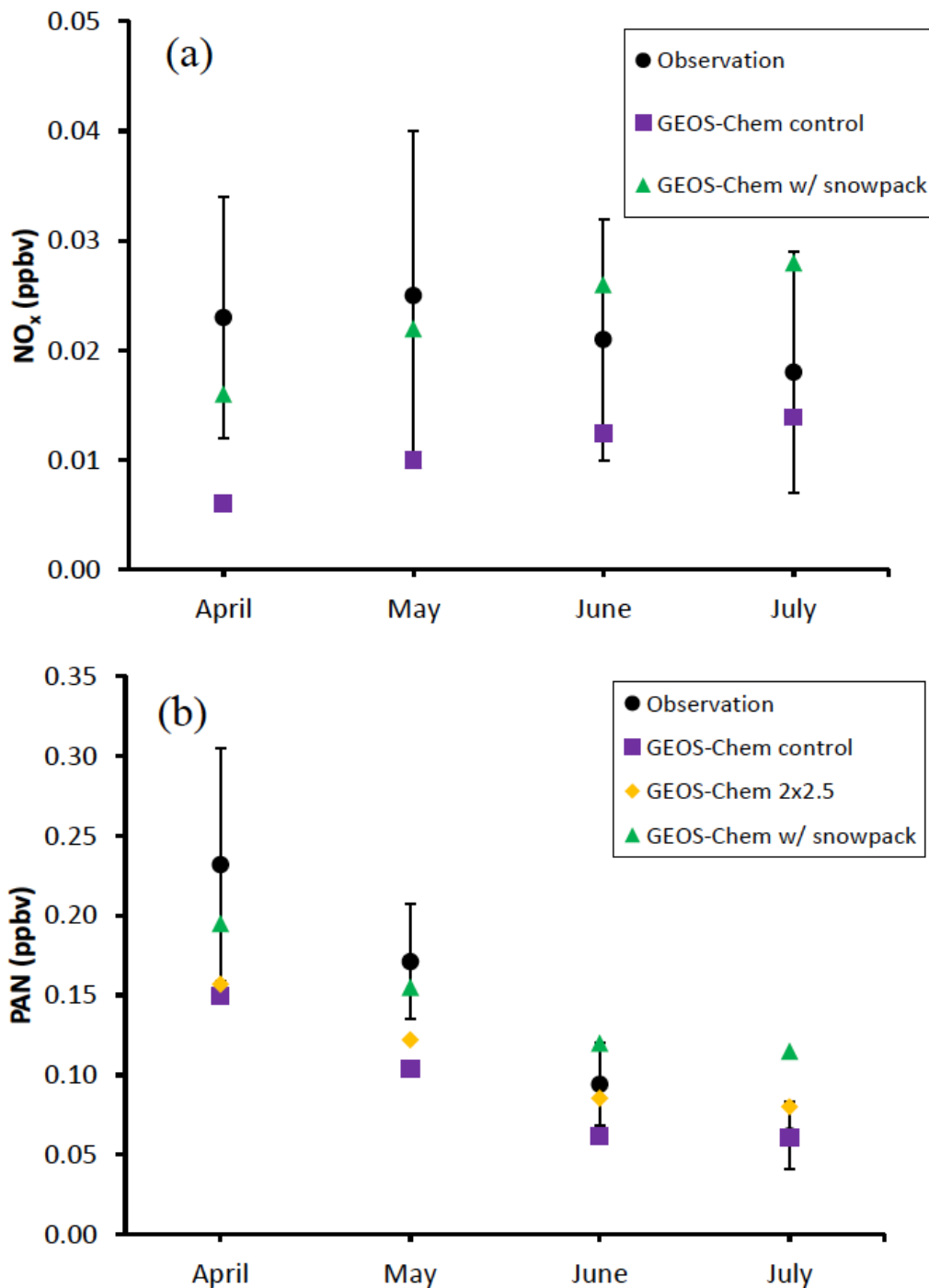
790



791

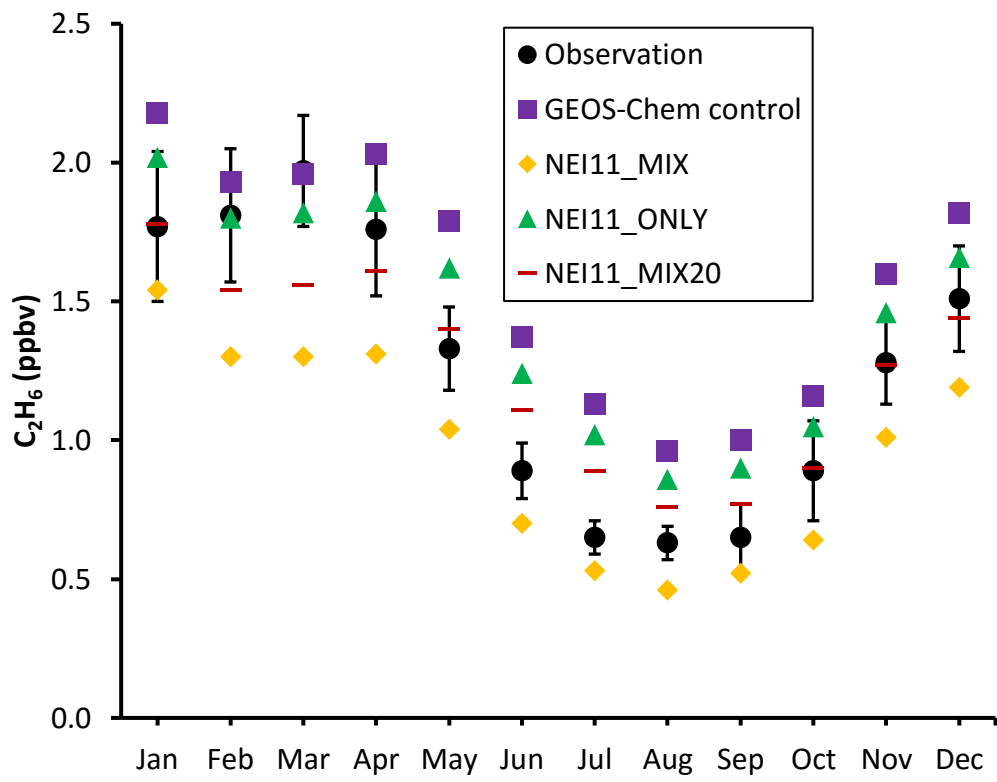
792 **Figure 3.** Scatter plots of model simulations from (a) GEOS-Chem control simulations and (b)
 793 EURO_EDGAR during 2009/12/01-2010/01/31 and measured monthly mean NO₂ mixing ratios
 794 at 11 observational sites over Europe; also shown are the corresponding model-to-observation
 795 slopes (k) and correlation coefficients (r) for each panel. The dashed line is the 1:1 ratio.
 796 Explanations of site abbreviations are listed in Table 1. EURO_EDGAR represents simulations
 797 with anthropogenic NO_x emissions over Europe following EDGAR v4.2, with other model
 798 configurations identical to the control simulations.

799



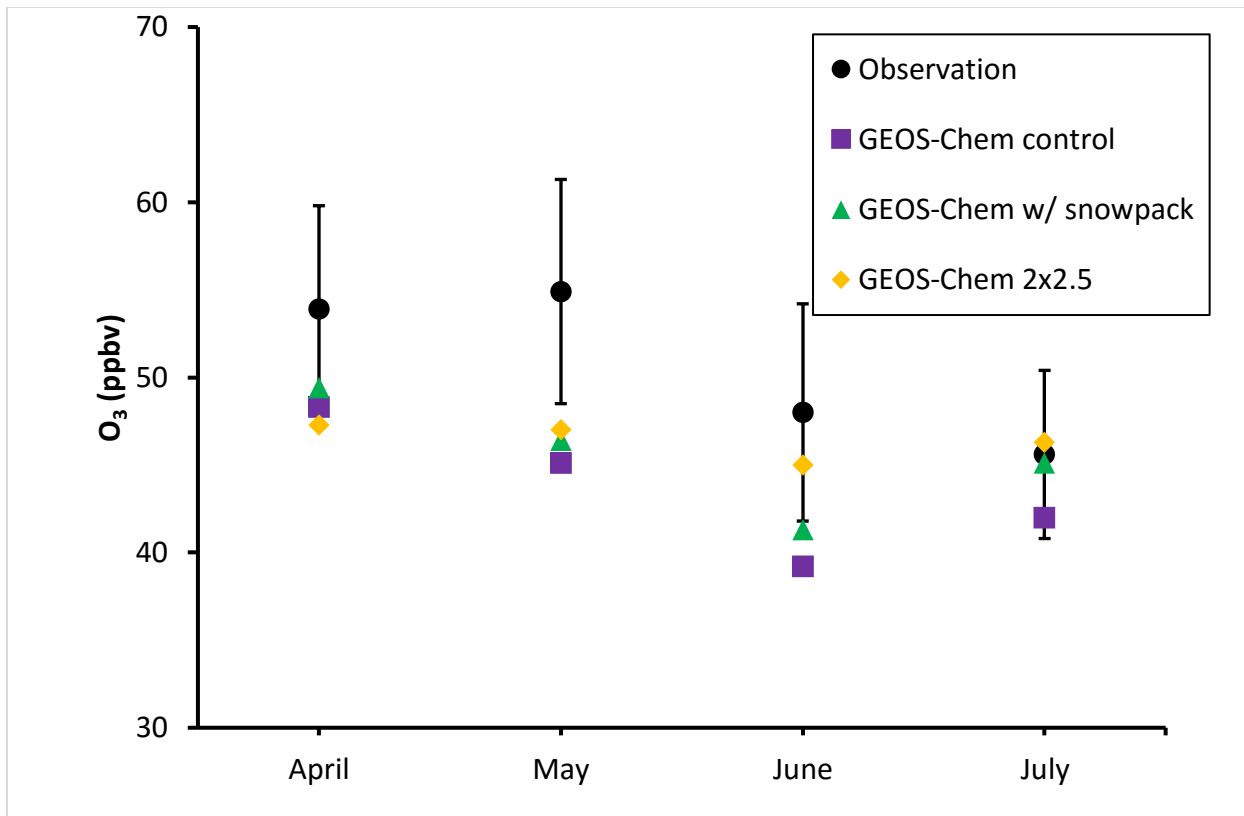
800

801 **Figure 4.** Monthly mean surface (a) NO_x and (b) PAN mixing ratios from observations (black
 802 circles), simulations with (green triangles) /without (purple squares) snowpack emissions, and
 803 GEOS-Chem simulations with horizontal grid resolution 2° x 2.5° (orange diamonds) for April-
 804 July during 07/2008-06/2010. Vertical bars denote standard deviations over the course of
 805 observations for each month.



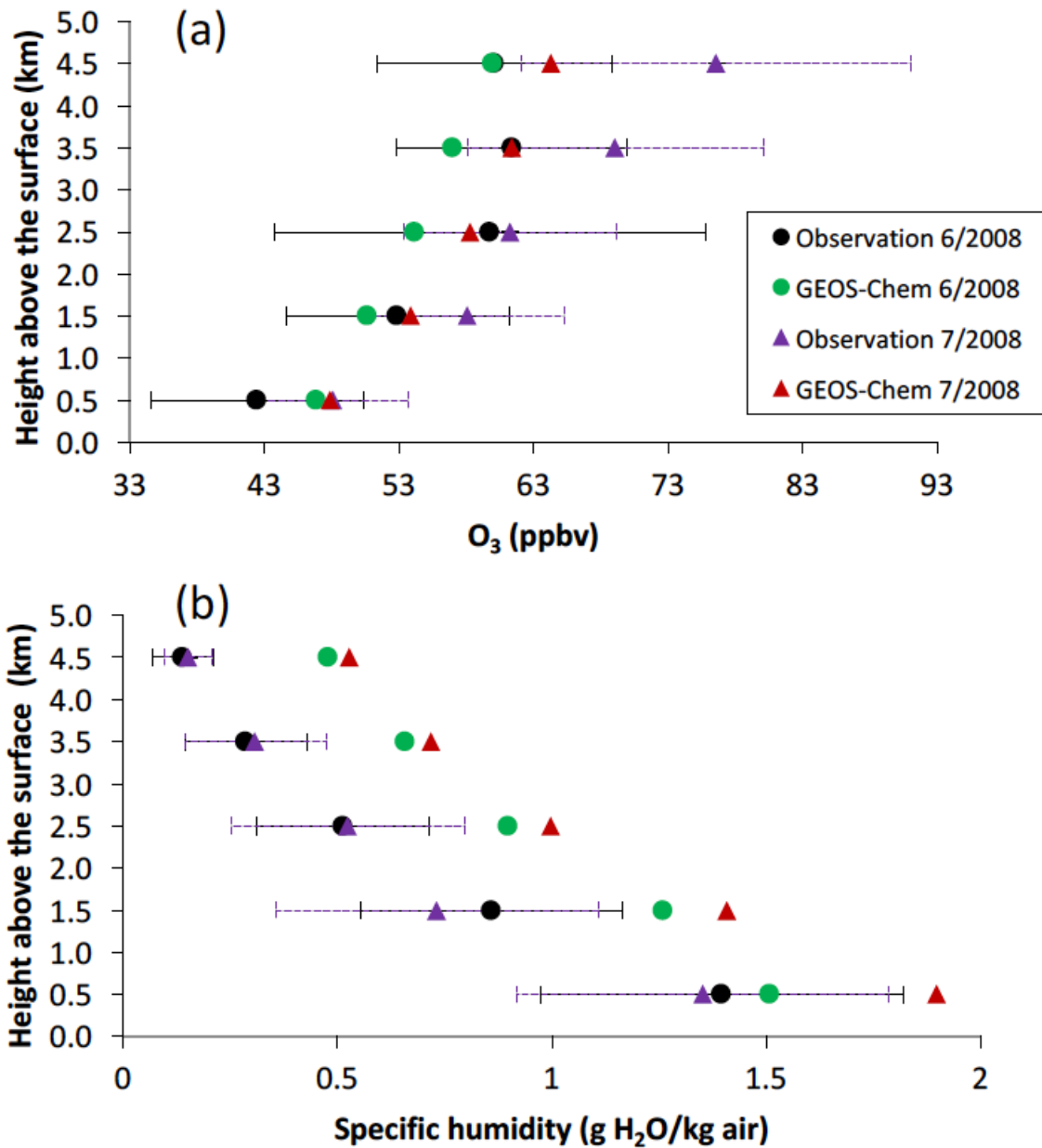
806
 807 **Figure 5.** Monthly mean surface C₂H₆ mixing ratios at Summit from observations (black
 808 circles), GEOS-Chem model control simulations (purple squares), NEI11_MIX (orange
 809 diamond), and NEI11_ONLY (green triangles) simulations during 2008-2010; vertical bars
 810 denote the standard deviation over the course of observations for each month. NEI11_MIX
 811 represents model perturbations with global C₂H₆ emission inventories overwritten by NEI11 over
 812 US and by MIX over Asia, with other model configurations identical to the control simulations.
 813 NEI11_ONLY denotes the simulation that is the same as the control simulation, except that the
 814 C₂H₆ emission inventory over the US is overwritten by NEI11. NEI11_MIX20 is the simulation
 815 that is identical to NEI11_MIX except for the 20% increased MIX C₂H₆ emission inventory over
 816 Asia.

817
 818
 819
 820



821
 822 **Figure 6.** Monthly mean surface O₃ mixing ratios from observations (black circles), GEOS-
 823 Chem control runs (purple squares), with snowpack chemistry (green triangles), and horizontal
 824 grid resolution 2° x 2.5° (orange diamonds) for April-July. Vertical bars denote the variability
 825 over the course of observations for each month.

826
 827
 828
 829
 830
 831
 832
 833



834

835 **Figure 7.** Comparisons of vertical profiles of (a) O₃ and (b) specific humidity between GEOS-
 836 Chem simulations and ozonesondes in June and July 2008 respectively, averaged over 1-km
 837 altitude bins. Black and green solid circles represent observations and simulations in June 2008,
 838 while purple and red triangles denote observations and simulations for July 2008. Solid and
 839 dashed horizontal error bars represent observational standard deviations for June and July,
 840 respectively.

841